3D Simulations Capture the Persistent Low-Mode Asymmetries Evident in Laser-Direct-Drive Implosions on OMEGA

A. Colaïtis*
Centre Lasers Intenses et Applications, UMR 5107, 351 Cours de la libération, 33400 Talence, France

D. P. Turnbull, I. V. Igumenschev, D. Edgell, R. C. Shah, O. M. Mannion, C. Stoeckl, D. Jacob-Perkins, A. Shvydky, R. Janezic, A. Kalb, D. Cao, C. J. Forrest, J. Kwiatkowski, S. Regan, W. Theobald, V. N. Goncharov, and D. H. Froula
Laboratory for Laser Energetics, 250 East River Road, Rochester, New York 14623-1212, USA

(Received 15 March 2022; revised 30 June 2022; accepted 25 July 2022; published 22 August 2022)

Spherical implosions in inertial confinement fusion are inherently sensitive to perturbations that may arise from experimental constraints and errors. Control and mitigation of low-mode (long wavelength) perturbations is a key milestone to improving implosion performances. We present the first 3D radiation-hydrodynamic simulations of directly driven inertial confinement fusion implosions with an inline package for polarized crossed-beam energy transfer. Simulations match bang times, yields (separately accounting for laser-induced high modes and fuel age), hot spot flow velocities and direction, for which polarized crossed-beam energy transfer contributes to the systematic flow orientation evident in the OMEGA implosion database. Current levels of beam mispointing, imbalance, target offset, and asymmetry from polarized crossed-beam energy transfer degrade yields by more than 40%. The effectiveness of two mitigation strategies for low modes is explored.

DOI: 10.1103/PhysRevLett.129.095001

Spherical implosion experiments in inertial confinement fusion (ICF) are notoriously prone to perturbations during the compression phase, which significantly degrade performances and can prevent target ignition. These may arise from target defects, small-scale structure in the intensity profile of the laser, and other experimental constraints and errors. Control and mitigation of low-mode (long wavelength) perturbations is a key milestone to improving implosion performances, be it in indirect-drive (ID) [1–5] or direct-drive (DD) configurations [6–8]. In experiments, many different sources of low modes may contribute to the final hot spot shape. It is therefore key to understanding the relative contributions and sensitivity of each low-mode source in order to guide future progress.

Simulation tools are valuable in exploring such dependencies. In order to explore the parameter space with any credibility, these tools must at least reproduce current experiments without relying on overtuning of the physics models. Recently, full 3D simulations for ID ICF have shown promise in approaching experimental data related to the fusing hot-spot characteristics and have successfully guided subsequent designs [9]. However, these tools are not adapted to some of the specific physics of DD ICF; self-amplified cross-beam energy transfer (CBET) between many beams, presence of laser caustics [10], statistical noise in computing reflected fields, etc. Recently, a 3D laser model specifically formulated for such physics, IFRIIT [11], was implemented inline [12] in the ASTER radiation hydrodynamics code [13,14].

In this Letter, we present the first 3D hydrodynamic simulations with sufficient physics models included to reproduce and quantify the anomalies observed in direct-drive implosions on OMEGA [15] without relying on *ad hoc* parameters. This is a significant step forward in understanding the key physics processes required for credible and robust DD ICF simulations. These simulations notably rely on a new physics formulation for CBET in ASTER/IFRIIT that include the physics of polarization transport and CBET-induced polarization rotation and birefringence. When including all the known effects (polarized CBET, mispointing, target offsets, beam power balance), the simulations reproduce the observables (bang times, yields, hot-spot velocity magnitude and direction). These integrated simulations are used to assess the effect of polarization through CBET and to explore the sensitivity of current direct-drive experiments to the various low-mode sources. In addition, the modeling is applied to current and prospective low-mode mitigation techniques, namely, low-mode compensation by target offset and redesign of the OMEGA polarization smoothing system, with the goal of assessing their respective limits and effectiveness.

In the past two years, a systematic low-mode asymmetry was noticed in ICF implosion experiments performed on OMEGA (a detailed study will be published based on Refs. [7,16]). This low-mode anomaly was observed in neutron time of flight diagnostics [7,17,18] which measured the neutron averaged velocity of the hot fusing plasma in these experiments. In an ideal implosion, this

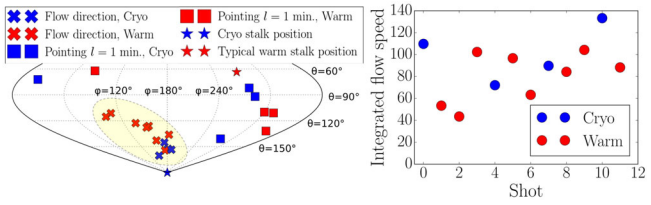

FIG. 1. Systematic flow direction shown in a sinusoidal projection of the OMEGA chamber (left) and associated velocity magnitude (right) in best-setup implosions [7,16]. The squares in the left plot indicate the preferential direction induced by the pointing error.

flow velocity is zero as the compression is symmetric, while here, systematic anomalies of the order of 80 km/s were observed. The associated flow direction appears to be systematically clustered in the southern hemisphere region [Fig. 1]. These anomalies were observed for experiments in the current best laser-performances for OMEGA: target offset less than 5 μm from the target chamber center, and beam pointing and imbalance with spherical harmonics amplitudes of modes $l=1$ and $l=2$ less than 2%. The anomaly remains clustered in the same angular region despite drastically different stalk positions between the warm and cryogenic experiments. This weak stalk-induced flow direction anomaly is also supported by experimental investigations presented in Ref. [19].

In OMEGA implosion experiments, 60 beams are normally incident onto a spherical shell target. The beams are smoothed by phase plates that shape the intensity profile on target, smoothing by spectral dispersion (SSD) that moves the speckle pattern in time to reduce high-frequency imprint from the laser and mitigate laser plasma instabilities (LPIs), and distributed polarization rotators (DPR), which separate each beam into two subbeams with orthogonal polarizations to further reduce laser imprint and LPIs. The 60 beam ports cover the sphere in a regular pattern, such that the compression should be symmetric in the ideal case. However, the DPRs introduce a nonsymmetric 90 μm offset between the orthogonal polarizations within each beam. Recently, it was shown [20] that this polarization configuration, coupled with CBET, produces a systematic low-mode anomaly with significant amplitude. While the authors suggest that this could explain the aforementioned flow anomaly, this study was performed on the basis of postprocessing, and did not account for the combined effects of other low-mode sources; such as target offset, beam imbalance, beam pointing error, as well as the dynamic coupling of polarized CBET with the target hydrodynamics. To account for this effect, our simulations model each subbeam created by the DPR system independently, i.e., 120 subbeams. Each subbeam was then decomposed onto an orthogonal basis to account for polarization effects. Finally, each field was decomposed into an incident and reflected field (so-called laser *sheets*) in order to account for beam self-amplification through CBET. In total, 480 complex fields in 3D were tracked for a full polarized CBET calculation, which represented a significant challenge computationally.

The inline polarization model proposed here was developed within the *field formulation* of geometrical optics (GO) implemented in IFRIIT [11]. The ray electric field was written $a = A\exp k_0\psi$, with k_0 the vacuum wave number, A the component of field amplitude due to refraction, and ψ a phase which accounts for absorption and energy exchange. The caustic fields were described using an etalon integral method (see Ref. [21], Sec. 3.5), assuming caustics of the form relevant to DD ICF [22]. The reconstructed field combines the expected Airy function of a locally linear density profile with a derivative of an Airy function that accounts for deviations from linearity in the profile and for caustic curvature. Most importantly, this reconstruction relies on rays only and does not introduce free parameters, contrary to what is commonly used in direct-drive CBET models to either limit caustic fields or tune the CBET interaction [23–26]. The ray field was then described onto the Frenet reference frame [27], an orthogonal basis associated with the ray and defined at every point by a tangent $\mathbf{l} = \mathbf{k}/|\mathbf{k}|$, a normal $\boldsymbol{\nu}$ parallel to the logarithmic gradient of the permittivity transverse to the ray, and a binormal $\mathbf{b} = \mathbf{l}\times\boldsymbol{\nu}$. The Frenet frame rotates with the ray, which allows us to account for polarization transport through refraction. The exchange of amplitude between the ray field components in the Frenet frame, denoted $(A_n)^T = (a_{n,\nu_n}, a_{n,b_n})$ for field n, can be written $\partial_{\mathbf{l}_n} A_n = \underline{\underline{\mathcal{D}_n}} A_n$ with $\underline{\underline{\mathcal{D}_n}}$ a matrix factoring the plasma response and the sheets contributions to amplification and polarization rotation (see the Appendix A). In the final model, the ray amplitude A is computed according to ray theory from a single inverse ray-tracing step [28], while the ray phase is obtained by integrating the permittivity along the ray trajectory, $\psi = \int \epsilon''[\mathbf{r}(\hat{\tau})]d\hat{\tau}/2$, where the permittivity components in the Frenet frame are

$$\begin{pmatrix} \epsilon_{n,\nu_n} \\ \epsilon_{n,b_n} \end{pmatrix} = [\epsilon'_n + \imath(\epsilon''_{0,n} f_L + \underline{\underline{\mathcal{D}_n}})] \cdot \begin{pmatrix} 1 \\ 1 \end{pmatrix}, \qquad (1)$$

with f_L a Langdon effect coefficient [12,29] and $\epsilon''_{0,n}$ accounts for collisional absorption. Pump depletion is obtained by iterating the ray phase computation until convergence.

Aside from the polarization physics and handling of caustics, the CBET model also differs from the usual implementations for ID ICF [30] by the addition of flow-induced frequency shift [31], and accounting for CBET between laser fields within the same beam and separated by turning points (i.e., self-amplification). We also account for the Langdon effect on ion acoustic waves [32], a physics effect not included in other DD ICF models but that is not a large factor here [12]. The polarized CBET

TABLE I. Summary of shot characteristics and low-mode system amplitude for the simulated experiments. The knowledge of the offset for 94712 (marked by a star) is uncertain due to a diagnostics issue—hence, the offset is not modeled for 94712. Neutron yields are corrected for fuel aging (tritium decay, 3He contamination and radiological capsule damage), with a factor of 0.59 for 94712 and 0.61 for 94343 [8].

						Balance $l = 1$ (% rms)				
Shot number	Date	E_{las} (kJ)	D_t (μm)	Offset (μm)	Pointing $l = 1$ (% rms)	Picket	Early drive	Late drive	Neutron yield Y_n (10^{14})	V_{flow} (km/s)
94343	09/07/2019	27.7	982.0	3.5	1.26	2.58	0.48	1.45	1.22 ± 0.052	109.8 ± 14.5
94712	09/08/2019	28.4	961.4	7.0*	5.94	4.52	0.35	1.34	1.31 ± 0.054	146.3 ± 12.0

model itself was validated against academic test cases and against the BeamletCrosser postprocessor [20,33] and is now used in inline 3D ASTER/IFRIIT [12,14] simulations.

The 3D modeling was applied to two OMEGA implosion experiments reported in Table I (see also the Appendix B). Shot 94343 is a cryogenic implosion typical of the best OMEGA laser performances, with low offset, pointing and balance error. We also consider shot 94712, a cryogenic implosion which had poor beam pointing due to issues with the initial laser alignment [7]. These two shots have slightly different target diameters, as part of a mitigation strategy for CBET [34]. For both shots, we conduct an extensive set of simulations while varying the CBET model and/or the number of low-mode sources that are included. The CBET model was toggled from off, to the commonly used *unpolarized* model [35] where the polarization effect for polarization-smoothed beams (e.g., DPR) is modeled with fixed polarization and without any rotation or ellipticity effects (see the Appendix A), to the fully polarized model presented here. The permutations of additional low modes are as follows: none (noted χ_0); measured individual beam power balance only (noted χ_B); beam power balance and measured individual beam pointing only (noted $\chi_{B,P}$); and beam power balance, pointing, and measured target offset (noted $\chi_{B,P,O}$). In all simulations, the Spitzer-Harm [36] heat conduction model was used at all time except in the first picket where the flux was limited with $f_{lim} = 0.1$ [13].

Several conclusions can be drawn from the simulation results for neutron data. (i) The CBET model alone gets nuclear bang time correctly, implying that the zero-order drive energetics is correct and well described by the model [Fig. 2(a)]. This also suggests that other effects not accounted here such as two plasmon decay do not significantly modify the total drive [37]. (ii) Unpolarized and polarized CBET simulations with power balance and pointing variations get the neutron yield correctly because both drive energetics and symmetry are important for the yield [Fig. 2(b)]. (iii) Both CBET models with power balance and pointing variations match the flow velocity correctly for shot 94712 [Fig. 2(c)], because the large pointing error dominates the low-mode sources. (iv) Polarized CBET with power balance and pointing is needed to get the flow velocity correctly for the more accurately pointed shot 94343 [Fig. 2(d)] (the low offset of 3.5 μm is seen to play a minor role). This indicates that the polarization effect begins to be more important as other low mode sources become smaller.

While there is a remaining discrepancy on the flow direction, here it must be emphasized that the laser pointing itself is challenging to characterize, which was recently demonstrated with two pointing shots 98754 and 98757 carried out in the morning and evening of the same day. These showed the $l = 1$ pointing direction changed by 80 to 115 degrees over the course of the day. The source of this

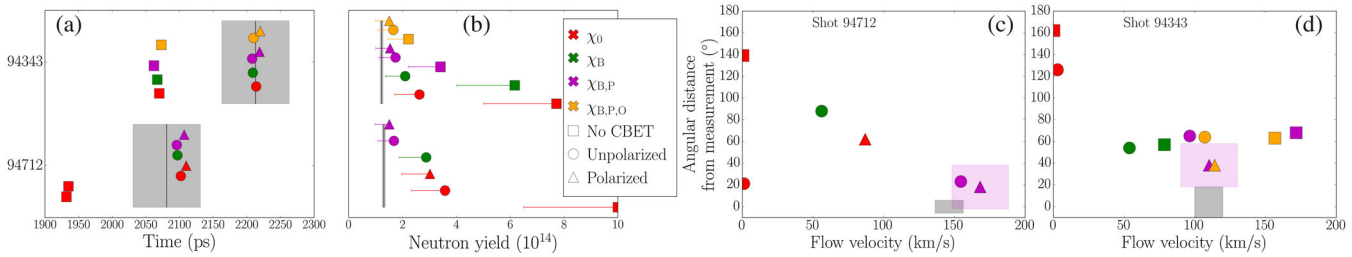

FIG. 2. Comparison of the simulated (colored symbols) and measured (gray shaded areas) bang time (a), neutron yield (b), flow velocity magnitude and angular distance from measurement (c),(d). The error bars on the simulated neutron yield estimate the effect from higher modes ($l = 64$ to 128) as a yield drop of ~30%, obtained from higher resolution simulations with the same model [38]. Experimental yields are corrected for tritium aging [8]. The purple-shaded area in (c),(d) is the estimated simulation uncertainty related to the knowledge of the pointing data, only highlighted for polarized CBET simulations in $\chi_{B,P}$. No simulations $\chi_{B,P,O}$ are conducted for 94712 due to low confidence in the offset measurement.

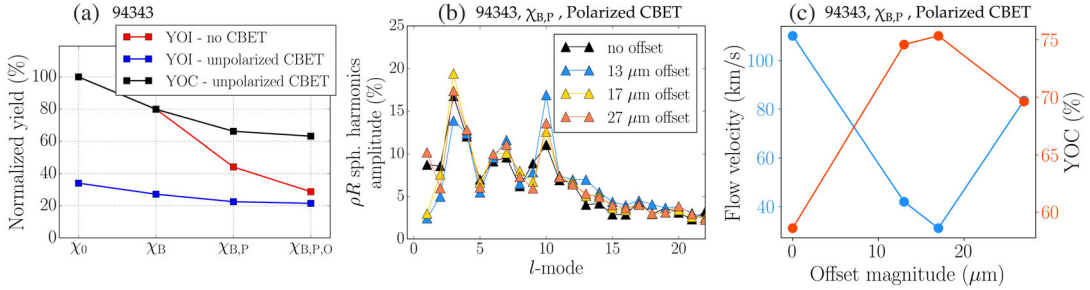

FIG. 3. (a) Scaling of the YOI (yield over case χ_0 in absence of CBET) and YOC (yield over case χ_0 in presence of CBET) for simulations with and without unpolarized CBET, as a function of low-mode asymmetry sources. (b) Amplitude of spherical harmonics modes of the target ρR at bang time for case $\chi_{B,P}$ and as a function of target offset along the initial flow direction. (c) Flow anomaly (blue) and YOC (red) as a function of offset magnitude for the same case as (b).

change may be related to two diagnostic transactions in the ten-inch manipulators (TIMs [39]). In addition, different analysis of the same pointing data can yield results that vary by 20°–60° when the $l = 1$ rms value is small (of the order of 1%–2%). For these reasons, the accurate knowledge of the pointing modes is limited. Calculations of the same shots using various pointing data suggest that the resulting flow direction can change in the 10°–40° range and the velocity magnitude by ∼20 km/s [38]. For this reason, 20° and 20 km/s uncertainties were added for the flow direction and magnitude on the simulation results given in Figs. 2(c) and 2(d).

The level of agreement between the simulation and the data provides confidence in the modeling tools, which in turn allows the exploration of the sensitivity of the implosions to various low modes. Here, it is useful to define normalized yields. We introduce the yield over ideal (YOI) as the yield over that of the 3D ideal case without CBET, and the yield over clean (YOC) as the yield over that of the 3D ideal case with unpolarized CBET. Examining the various cases, the simulations suggest that OMEGA implosions lose ∼40% in YOC due to effects of balance, pointing and offset alone [Fig. 3(a)]. In addition, the effect of unpolarized CBET alone reduces the YOI by ∼65% through loss of coupling. In that framework, the polarization effect of CBET only causes a drop of an additional 6% YOC. Here, the various combinations of perturbations, including the polarization physics, can trade off, leaving rather similar performance albeit for slightly different combinations of input. This generally consistent performance is a hallmark of rigorous examination of the cryogenic implosion database [40]. However, with ideal pointing and balance, the polarized CBET alone reduces the YOC by 18% and induces ∼90 km/s flow anomaly compared to an unpolarized CBET case, which shows that this anomaly should ultimately be mitigated.

Volume maps of the compressed target shape near peak neutron production for the more accurately pointed shot 94343 are given in Figs. 4(a)–4(d). The ideal compression cases feature a symmetric shell and hot-spot shape [Figs. 4(a) and 4(b)], while adding the system-induced low modes lead to an asymmetric and distorted compression [Figs. 4(c)–4(d)]. Examining the modal decomposition of areal density near stagnation in the absence of CBET [Fig. 4(e)], the effect of energy balance for 94343 is in the range of 5%–10% rms for low modes—which almost punctures the target—while adding the effect of pointing increases the low-mode perturbation to 10%–15% and clearly leads to target perforation [Fig. 4(d)]. Adding the effect of unpolarized CBET [Fig. 4(f)], these low-mode perturbations decrease back to the 5%–10% range [41] even when accounting for pointing and energy balance. However, the mode $l = 10$, characteristic of CBET on OMEGA [33], increases by a factor of 2 to 3 up to 30% rms, which leads to a symmetric target perforation pattern [Fig. 4(b)]. This amplification was also seen when considering pointing and balance in addition to CBET, although the absolute value reached was here of the order of 15%. This is a 3D consequence of CBET in the 60 beam geometry and may contribute to the unexplained scaling of beam-target size in detailed statistical examination of the OMEGA cryogenic database [8].

We now explore the effectiveness of two different strategies to mitigate low-mode asymmetries in laser direct drive implosions. The first strategy utilizes a prescribed target offset to intentionally compensate for the inherent laser mode-one asymmetry [42] in the direction opposite to the flow. This method is routinely used in OMEGA experiment to improve yield between shots, and we explore here the extent to which this approach can be useful. The second strategy involves updating the DPRs used on OMEGA to mitigate the polarization asymmetry. This strategy was proposed in Ref. [20] on the basis of postprocessing simulations. To compare these two strategies, simulations were performed for shot 94343 in $\chi_{B,P}$ with polarized CBET.

Simulations for the offset strategy were performed with compensations ranging from 13 to 27 μm, as suggested by the literature [7]. Figure 3(c) shows the YOC increases from 58.5% in the no-offset case to ∼75% in the 17 μm case. The trend indicates a saturation effect with a flattening

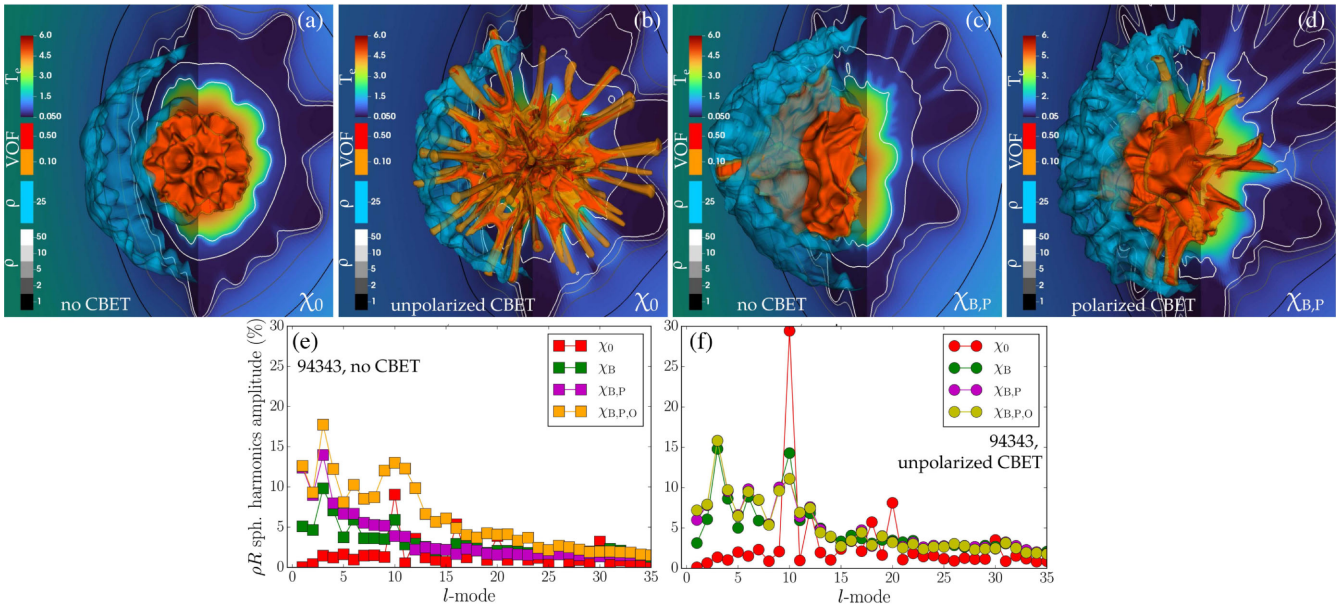

FIG. 4. (a–d) Target hot-spot electron temperature (colored background, kilo-electron-volts), 10% and 50% volume fraction of DT gas (orange and red volume contours, respectively), 25 g/cc density isovalue (light blue volume contour), and 1, 2, 5, 10 and 50 g/cc isocontours (black to white contour lines). (e,f) Amplitude of spherical harmonics modes of the shell ρR for various low-mode sources, without CBET (e) and with unpolarized CBET (f). All figures are taken at bang time and for shot 94343.

of the YOC curve around the maximum, due to higher modes not being mitigated by a simple offset—notably, polarized CBET induces l modes up to $l = 4$ [33]. Simulations performed with the revised DPR system used a 10 μm spot offset and half the SSD bandwidth of the original system. In that configuration, the two subbeams from the DPR nearly overlap and were nearly round. Simulations of polarized CBET for $\chi_{B,P}$ give results close to an unpolarized case both in terms of flow direction and magnitude, to within 5° for the flow direction and 7 km/s for the flow velocity. Here, the yield does not increase, because only the CBET anomaly was corrected and the imbalance and pointing errors are still present and of the same order of magnitude in importance. However, the recovery of the unpolarized results suggests that this strategy would be more effective in the long term, since implosions would not be limited in yield by the higher modes from polarized CBET.

In conclusion, we have developed a new, inline-capable 3D model for treating the energy exchange between polarized beams. Applied to simulations of cryogenic OMEGA implosions, the model reproduces the bang time, neutron yield, flow velocity and direction of two cryogenic shots without setting *ad hoc* parameters, within the uncertainties of laser pointing and accounting for fuel aging (tritium decay, 3He contamination and radiological capsule damage) and laser-induced high modes. Notably, the polarized CBET model reproduces the systematic flow direction observed across many shots conducted in the last years. Investigation of various cases highlight how low modes degrade the YOC by ∼40%. CBET itself reduces the YOI by ∼80% and tends to puncture targets through mode $l = 10$. Low-mode mitigation using target offset was shown to saturate rapidly due to the variety of low modes induced by the compounded effect of beam power balance, pointing and polarized CBET. Conversely, a redesigned DPR system with lower spot offset was investigated and shows that it can recover the unpolarized CBET results, thus removing the systematic flow anomaly.

This work was granted access to the HPC resources of TGCC under the allocations 2020-A0070506129, 2021-A0090506129 made by GENCI, and PRACE Grant No. 2021240055. This work has been carried out within the framework of the EUROfusion Consortium, funded by the European Union via the Euratom Research and Training Programme (Grant Agreement No. 101052200–EUROfusion). Views and opinions expressed are, however, those of the author(s) only and do not necessarily reflect those of the European Union or the European Commission. Neither the European Union nor the European Commission can be held responsible for them. The involved teams have operated within the framework of the Enabling Research Project: ENR-IFE.01.CEA "Advancing shock ignition for direct-drive inertial fusion." The software used in this work was developed in part at the University of Rochester's Laboratory for Laser Energetics. This material is based upon work supported by the Department of Energy National Nuclear Security Administration under Award No. DE-NA0003856, the University of Rochester, and the New York State Energy Research and Development Authority.

Appendix A: The polarized CBET matrix coefficients.—The coupling of the ray sheet components is written in the Frenet frame, which is transported along the ray and rotates with refraction. Here, we assume that the additional frame rotation from ray torsion [27], an effect related to the second order derivative of the permittivity profile, can be neglected. This approximation is reasonable for DD ICF, since the ray torsion is zero by definition in spherically layered profiles. The Frenet frame field components are coupled with each other and with the plasma through a formulation that reduces to $\partial_{\mathbf{l_n}} A_n = \underline{\underline{\mathcal{D}_n}} A_n$, where $\underline{\underline{\mathcal{D}_n}}$ reads

$$\underline{\underline{\mathcal{D}_n}} = \frac{\iota}{8k_n} \sum_{\substack{m\in\text{beams,sheets} \\ m\neq n}}^{N} K^{\star}_{nm} k^2_{b,nm} \begin{pmatrix} a^2_{m,\nu_n} & a^{\star}_{m,b_n} a_{m,\nu_n} \\ a_{m,b_n} a^{\star}_{m,\nu_n} & a^2_{m,b_n} \end{pmatrix}, \tag{A1}$$

where the subscripts n and m refer to quantities of ray fields n and m, respectively, a_{m,ν_n} and a_{m,b_n} are the components of field m projected onto the Frenet frame of field n ($\boldsymbol{\nu}_n$ and $\mathbf{b}_n$, respectively), $K^{\star}_{nm} = K_{mn} = \chi_e(1+\chi_i)/(1+\chi_e+\chi_i)$ is the plasma response function, with χ_e and χ_i the electron and ion dielectric susceptibilities, respectively, which argument depends notably on the k_i and ω_i, the beat-wave wave number is $k_{b,nm} = |\mathbf{k}_n - \mathbf{k}_m|$, and the summation for $\underline{\underline{\mathcal{D}_n}}$ is carried over all laser sheets except n.

Here, the plasma response function K is complex valued, with the imaginary part responsible for depletion or gain and the real part responsible for inducing ellipticity in the system. In addition, the matrix in Eq. (A1) accounts for both ellipticity and rotating the probe beam polarization toward that of the pump. Finally, since the model is written in the ray Frenet frame, it also accounts for polarization rotation due to refraction. By contrast, the *unpolarized* CBET model described in Ref. [35] and usually employed in inline CBET modeling only describes the field component a_{m,ν_n}, assuming it is real valued and accounting for an average effect of polarization. This unpolarized model was derived assuming a polarization smoothing system where each beam contains half of its power in two orthogonal polarization components which are static. This approach yields $a^2_{m,\nu_n} = (1+\cos^2\Theta_{mn})a^2_m/4$ with Θ_{mn} the angle between the k vectors of fields m and n. This approach neglects polarization rotation through refraction, polarization rotation due to pump-probe interaction, and ellipticity induced in the beams through the interaction with the CBET-induced plasma perturbations.

The multisheet coupling and pump depletion is obtained by iterating the integration of the ray phase along trajectories, thus updating the coupling coefficient in $\underline{\underline{\mathcal{D}_n}}$. In the real-valued GO framework [27,28], the etalon integral does not depend on the imaginary part of the ray phase. As such, caustic fields are simply updated each time the ray phase is recomputed when iterating the CBET coefficients for pump depletion. At iteration convergence, and for the highest intensities at play here, the energy conservation is typically ~0.2% of the incident energy and ~1% of the exchanged energy (see Ref. [12]).

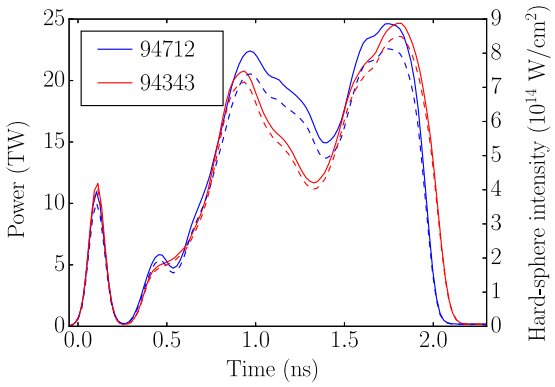

FIG. 5. Nominal pulse shapes used for shots 94712 (blue) and 94343 (red). The solid line indicates the power profile and the dashed lines the corresponding average laser intensity computed on a hard sphere at the initial target surface.

Appendix B: The setup of shots 94343 and 94712.—In this Letter, we consider two cryogenic shots numbered 94343 and 94712. Both implosions were carried out in a standard setup for OMEGA, with 60 beams equipped with SG5 phase plates, DPR system, and SSD. Using the full smoothing capabilities, the SG5 phase plates produce laser spots of super-Gaussian shape of order 5.2 with a $1/e$ radius of 358 μm. A detailed description of the DPR spot configuration is given in Ref. [33]. For the SG5 phase plates, the radius encircling 95% of the beam energy is of 430 μm. Given the initial target diameters reported in Table I, the corresponding beam radius over target radius are of 87.6% and 89.5% for 94343 and 94712, respectively.

The pulse shapes employed for both shots are given in Fig. 5. They are constituted of an initial picket used to set the target adiabat, followed by a main drive pulse separated by a small dip. These typical pulses were obtained through a 1D machine learning optimization campaign [40].

*arnaud.colaitis@u-bordeaux.fr

[1] Hans G. Rinderknecht, D. T. Casey, R. Hatarik, R. M. Bionta, B. J. MacGowan, P. Patel, O. L. Landen, E. P. Hartouni, and O. A. Hurricane, Azimuthal Drive Asymmetry in Inertial Confinement Fusion Implosions on the National Ignition Facility, Phys. Rev. Lett. **124**, 145002 (2020).

[2] D. T. Casey *et al.*, Evidence of Three-Dimensional Asymmetries Seeded by High-Density Carbon-Ablator Nonuniformity in Experiments at the National Ignition Facility, Phys. Rev. Lett. **126**, 025002 (2021).

[3] D. J. Schlossberg *et al.*, Observation of Hydrodynamic Flows in Imploding Fusion Plasmas on the National Ignition Facility, Phys. Rev. Lett. **127**, 125001 (2021).
[4] A. B. Zylstra *et al.*, Record Energetics for an Inertial Fusion Implosion at NIF, Phys. Rev. Lett. **126**, 025001 (2021).
[5] O. A. Hurricane, D. T. Casey, O. Landen, D. A. Callahan, R. Bionta, S. Haan, A. L. Kritcher, R. Nora, P. K. Patel, P. T. Springer, and A. Zylstra, Extensions of a classical mechanics "piston model" for understanding the impact of asymmetry on ICF implosions: The cases of mode 2, mode 2/1 coupling, time-dependent asymmetry, and the relationship to coast time, Phys. Plasmas **29**, 012703 (2022).
[6] D. T. Michel, I. V. Igumenshchev, A. K. Davis, D. H. Edgell, D. H. Froula, D. W. Jacobs-Perkins, V. N. Goncharov, S. P. Regan, A. Shvydky, and E. M. Campbell, Subpercent-Scale Control of 3D Low Modes of Targets Imploded in Direct-Drive Configuration on Omega, Phys. Rev. Lett. **120**, 125001 (2018).
[7] O. M. Mannion *et al.*, Mitigation of mode-one asymmetry in laser-direct-drive inertial confinement fusion implosions, Phys. Plasmas **28**, 042701 (2021).
[8] A. Lees *et al.*, Experimentally Inferred Fusion Yield Dependencies of Omega Inertial Confinement Fusion Implosions, Phys. Rev. Lett. **127**, 105001 (2021).
[9] D. S. Clark, C. R. Weber, J. L. Milovich, A. E. Pak, D. T. Casey, B. A. Hammel, D. D. Ho, O. S. Jones, J. M. Koning, A. L. Kritcher, M. M. Marinak, L. P. Masse, D. H. Munro, M. V. Patel, P. K. Patel, H. F. Robey, C. R. Schroeder, S. M. Sepke, and M. J. Edwards, Three-dimensional modeling and hydrodynamic scaling of national ignition facility implosions, Phys. Plasmas **26**, 050601 (2019).
[10] Regions of inapplicability of geometrical optics near ray turning points.
[11] A. Colaïtis, R. K. Follett, J. P. Palastro, I. Igumenschev, and V. Goncharov, Adaptive inverse ray-tracing for accurate and efficient modeling of cross beam energy transfer in hydrodynamics simulations, Phys. Plasmas **26**, 072706 (2019).
[12] A. Colaïtis, I. Igumenshchev, J. Mathiaud, and V. Goncharov, Inverse ray tracing on icosahedral tetrahedron grids for nonlinear laser plasma interaction coupled to 3D radiation hydrodynamics, J. Comput. Phys. **443**, 110537 (2021).
[13] I. V. Igumenshchev, V. N. Goncharov, F. J. Marshall, J. P. Knauer, E. M. Campbell, C. J. Forrest, D. H. Froula, V. Yu. Glebov, R. L. McCrory, S. P. Regan, T. C. Sangster, S. Skupsky, and C. Stoeckl, Three-dimensional modeling of direct-drive cryogenic implosions on omega, Phys. Plasmas **23**, 052702 (2016).
[14] I. V. Igumenshchev, D. T. Michel, R. C. Shah, E. M. Campbell, R. Epstein, C. J. Forrest, V. Yu. Glebov, V. N. Goncharov, J. P. Knauer, F. J. Marshall, R. L. McCrory, S. P. Regan, T. C. Sangster, C. Stoeckl, A. J. Schmitt, and S. Obenschain, Three-dimensional hydrodynamic simulations of omega implosions, Phys. Plasmas **24**, 056307 (2017).
[15] T. R. Boehly, D. L. Brown, R. S. Craxton, R. L. Keck, J. P. Knauer, J. H. Kelly, T. J. Kessler, S. A. Kumpan, S. J. Loucks, S. A. Letzring, F. J. Marshall, R. L. McCrory, S. F. B. Morse, W. Seka, J. M. Soures, and C. P. Verdon, Initial performance results of the OMEGA laser system, Opt. Commun. **133**, 495 (1997).
[16] S. P. Regan, O. M. Mannion, and C. J. Forrest, Systematic trends of hot-spot flow velocity in laser-direct-drive implosions on omega (2021), https://www.lle.rochester.edu/media/publications/presentations/documents/APS21/Regan_APS21.pdf.
[17] R. A. Lerche, L. W. Coleman, J. W. Houghton, D. R. Speck, and E. K. Storm, Laser fusion ion temperatures determined by neutron time of flight techniques, Appl. Phys. Lett. **31**, 645 (1977).
[18] R. Hatarik, D. B. Sayre, J. A. Caggiano, T. Phillips, M. J. Eckart, E. J. Bond, C. Cerjan, G. P. Grim, E. P. Hartouni, J. P. Knauer, J. M. Mcnaney, and D. H. Munro, Analysis of the neutron time-of-flight spectra from inertial confinement fusion experiments, J. Appl. Phys. **118**, 184502 (2015).
[19] M. Gatu Johnson *et al.*, Impact of stalk on directly driven inertial confinement fusion implosions, Phys. Plasmas **27**, 032704 (2020).
[20] D. H. Edgell, P. B. Radha, J. Katz, A. Shvydky, D. Turnbull, and D. H. Froula, Nonuniform Absorption and Scattered Light in Direct-Drive Implosions Driven by Polarization Smoothing, Phys. Rev. Lett. **127**, 075001 (2021).
[21] V. M. Babic and V. S. Buldyrev, *Short-Wavelength Diffraction Theory: Asymptotic Methods*, Springer Series on Wave Phenomena (Springer-Verlag, Berlin, 1972).
[22] Caustics of fold type, involving the degeneracy of 2 rays to a single solution.
[23] I. V. Igumenshchev, D. H. Edgell, V. N. Goncharov, J. A. Delettrez, A. V. Maximov, J. F. Myatt, W. Seka, A. Shvydky, S. Skupsky, and C. Stoeckl, Crossed-beam energy transfer in implosion experiments on omega, Phys. Plasmas **17**, 122708 (2010).
[24] J. A. Marozas *et al.*, Wavelength-detuning cross-beam energy transfer mitigation scheme for direct drive: Modeling and evidence from national ignition facility implosions, Phys. Plasmas **25**, 056314 (2018).
[25] D. H. Edgell, R. K. Follett, I. V. Igumenshchev, J. F. Myatt, J. G. Shaw, and D. H. Froula, Mitigation of cross-beam energy transfer in symmetric implosions on omega using wavelength detuning, Phys. Plasmas **24**, 062706 (2017).
[26] R. K. Follett, J. G. Shaw, J. F. Myatt, V. N. Goncharov, D. H. Edgell, D. H. Froula, and J. P. Palastro, Ray-based modeling of cross-beam energy transfer at caustics, Phys. Rev. E **98**, 043202 (2018).
[27] Y. A. Kravtsov and N. Y. Zhu, *Theory of Diffraction, Heuristic Approaches*, Alpha Science Series on Wave Phenomena (Alpha Science International Ltd, Oxford, U.K., 2010).
[28] A. Colaïtis, J. P. Palastro, R. K. Follett, I. V. Igumenschev, and V. Goncharov, Real and complex valued geometrical optics inverse ray-tracing for inline field calculations, Phys. Plasmas **26**, 032301 (2019).
[29] A. Bruce Langdon, Nonlinear Inverse Bremsstrahlung and Heated-Electron Distributions, Phys. Rev. Lett. **44**, 575 (1980).
[30] D. J. Strozzi, D. S. Bailey, P. Michel, L. Divol, S. M. Sepke, G. D. Kerbel, C. A. Thomas, J. E. Ralph, J. D. Moody, and M. B. Schneider, Interplay of Laser-Plasma Interactions and Inertial Fusion Hydrodynamics, Phys. Rev. Lett. **118**, 025002 (2017).

[31] T. Dewandre, J. R. Albritton, and E. A. Williams, Doppler shift of laser light reflected from expanding plasmas, Phys. Fluids **24**, 528 (1981).
[32] D. Turnbull, A. Colaïtis, A. M. Hansen, A. L. Milder, J. P. Palastro, J. Katz, C. Dorrer, B. E. Kruschwitz, D. J. Strozzi 2, and D. H. Froula, Impact of the Langdon effect on crossed-beam energy transfer, Nat. Phys. **16**, 181 (2020).
[33] A. Colaïtis *et al.*, 3D simulations of Inertial Confinement Fusion implosions part 1: Inline modeling of polarized cross beam energy transfer and subsequent drive anomalies on OMEGA and NIF (to be published).
[34] I. V. Igumenshchev, D. H. Froula, D. H. Edgell, V. N. Goncharov, T. J. Kessler, F. J. Marshall, R. L. McCrory, P. W. McKenty, D. D. Meyerhofer, D. T. Michel, T. C. Sangster, W. Seka, and S. Skupsky, Laser-Beam Zooming to Mitigate Crossed-Beam Energy Losses in Direct-Drive Implosions, Phys. Rev. Lett. **110**, 145001 (2013).
[35] P. Michel, L. Divol, E. A. Williams, C. A. Thomas, D. A. Callahan, S. Weber, S. W. Haan, J. D. Salmonson, N. B. Meezan, O. L. Landen, S. Dixit, D. E. Hinkel, M. J. Edwards, B. J. MacGowan, J. D. Lindl, S. H. Glenzer, and L. J. Suter, Energy transfer between laser beams crossing in ignition hohlraums, Phys. Plasmas **16**, 042702 (2009).
[36] L. Spitzer and R. Härm, Transport phenomena in a completely ionized gas, Phys. Rev. **89**, 977 (1953).
[37] D. Turnbull, A. V. Maximov, D. H. Edgell, W. Seka, R. K. Follett, J. P. Palastro, D. Cao, V. N. Goncharov, C. Stoeckl, and D. H. Froula, Anomalous Absorption by the Two-Plasmon Decay Instability, Phys. Rev. Lett. **124**, 185001 (2020).
[38] A. Colaïtis *et al.*, 3D simulations of Inertial Confinement Fusion implosions part 2: Systematic flow anomalies and impact of low modes on performances in OMEGA experiments (to be published).
[39] The TIM is a system used to position diagnostics near the target chamber center. See https://www.lle.rochester.edu/media/omega_facility/documentation/documents/S-AD-M-011Chap.7RevAfinal11-29-07.pdf.
[40] V. Gopalaswamy *et al.*, Tripled yield in direct-drive laser fusion through statistical modelling, Nature (London) **565**, 581 (2019).
[41] K. S. Anderson, C. J. Forrest, O. M. Mannion, F. J. Marshall, R. C. Shah, D. T. Michel, J. A. Marozas, P. B. Radha, D. H. Edgell, R. Epstein, V. N. Goncharov, J. P. Knauer, M. Gatu Johnson, and S. Laffite, Effect of cross-beam energy transfer on target-offset asymmetry in direct-drive inertial confinement fusion implosions, Phys. Plasmas **27**, 112713 (2020).
[42] O. M. Mannion, J. P. Knauer, V. Yu. Glebov, C. J. Forrest, A. Liu, Z. L. Mohamed, M. H. Romanofsky, T. C. Sangster, C. Stoeckl, and S. P. Regan, A suite of neutron time-of-flight detectors to measure hot-spot motion in direct-drive inertial confinement fusion experiments on omega, Nucl. Instrum. Methods Phys. Res., Sect. A **964**, 163774 (2020).